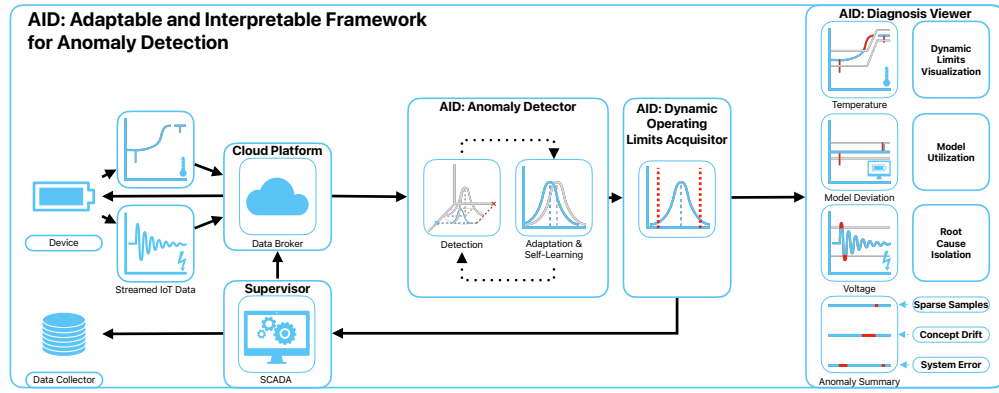


Graphical Abstract

Adaptable and Interpretable Framework for Anomaly Detection in SCADA-based IoT Systems

Marek Wadinger, Michal Kvasnica



Highlights

Adaptable and Interpretable Framework for Anomaly Detection in SCADA-based IoT Systems

Marek Wadinger, Michal Kvasnica

- Interpretable anomaly detector with self-supervised adaptation
- Delivers comparable performance to established general methods
- Isolates root cause of anomalies while considering interactions
- Demonstrates interpretability by providing operating limits for signals
- Uses self-learning approach on streamed IoT data

Adaptable and Interpretable Framework for Anomaly Detection in SCADA-based IoT Systems

Marek Wadinger^{a,b,*}, Michal Kvasnica^{a,b}

^a*Institute of Information Engineering, Automation and Mathematics, Slovak University of Technology in Bratislava, Radlinskeho 9, 812 37, Bratislava, Slovakia*

^b*Tesla 50Hz s.r.o., Pálenica 53/79, 033 17, Liptovský Hrádok, Slovakia*

Abstract

In this paper, we introduce an Adaptable and Interpretable Framework for Anomaly Detection (AID) designed for industrial systems utilizing IoT data streams on top of well-established SCADA systems. AID leverages dynamic conditional probability distribution modeling to capture the normal operation of dynamic systems and isolate the root causes of anomalies at the level of individual inputs. The self-supervised framework dynamically updates parameters of underlying model, allowing it to adapt to non-stationarity. AID interprets anomalies as significant deviations from conditional probability, encompassing interactions as well as both spatial and temporal irregularities by exposing them as features. Crucially, AID provides dynamic operating limits to integrate with existing alarm handling mechanisms in SCADA-based IoT systems. Two industrial-scale case studies demonstrate AID's capabilities. The first study showcases AID's effectiveness on energy storage system, adapting to changes, setting context-aware limits for SCADA, and ability to leverage a physical model. The second study monitors battery module temperatures, where AID identifies hardware faults, emphasizing its relevance to energy storage safety. A benchmark evaluation on real data shows that AID delivers comparable performance to other self-learning adaptable anomaly detection methods, with the significant advancement in diagnostic capabilities for improved system reliability and performance.

Keywords: Anomaly detection, Root cause isolation, Iterative learning,

*Phone numbers: +421 902 810 324 (Marek Wadinger)

Email addresses: marek.wadinger@stuba.sk (Marek Wadinger), michal.kvasnica@stuba.sk (Michal Kvasnica)

1. Introduction

Anomaly detection systems play a critical role in risk-averse systems by identifying abnormal patterns and adapting to novel expected patterns in data. These systems are particularly vital in the context of Internet of Things (IoT) devices that continuously stream high-fidelity data to control units.

In this rapidly evolving field with long-spanning roots, Chandola et al. (2009) conducted an influential review of prior research efforts across diverse application domains. Recent studies have underscored the need for holistic and tunable anomaly detection methods accessible to operators (Laptev et al., 2015; Kejariwal, 2015; Cook et al., 2020).

Cook et al. denote substantial aspects that pose challenges to anomaly detection in IoT, including the temporal, spatial, and external context of measurements, multivariate characteristics, noise, and nonstationarity (Cook et al., 2020). To address these complexity issues, Zhang et al. (2024) have successfully employed spatially distributed sensors and time-relative modulation. Their approach has proven effective, particularly in the context of complex non-linear systems, offering potential solutions to some of the challenges posed by IoT data. Huang et al., on the other hand, tackled the problems of detecting global outliers, local outliers, and outlier clusters simultaneously. Their proposed approach, based on density estimation, relies on the notion that density distributions should exhibit minimal variations in local areas. To achieve this, they introduce a novel turning ratio metric, which reduces reliance on hyperparameters and enhances anomaly detection (Huang et al., 2023).

Additionally, feature engineering techniques play a crucial role in capturing contextual properties and enhancing anomaly detection performance (Fan et al., 2019). However, it is worth noting that feature engineering may introduce categorical variables and significantly increase the dimensionality of the data, requiring specific methods for handling large data, sizeable data storage, and substantial computational resources (Talagala et al., 2021). Recently, Li et al. introduced an attribute-weighted outlier detection algorithm, designed for high-dimensional datasets with mixtures of categorical and numerical data. Their approach assigns different weights to individual attributes based on their importance in anomaly detection and uses

35 these weights to calculate distances between data points. Notably, Li et
36 al. demonstrated the superior performance of their algorithm compared to
37 state-of-the-art methods (Li and Liu, 2024). Another strategy for handling
38 high-dimensional data involves using deep learning methods with synthetic
39 normal data to enhance the detection of outliers with subtle deviations, as
40 proposed in Du et al. (2024).

41 Nevertheless, the presence of nonstationarity, often stemming from con-
42 cept drift (a shift in data patterns due to changes in statistical distribution)
43 and change points (permanent alterations in system state), presents a sub-
44 stantial challenge (Salehi and Rashidi, 2018). In practical scenarios, those
45 changes tend to be unpredictable in both their spatial and temporal aspects.
46 Consequently, they require systems with solid outlier rejection capabilities of
47 intelligent tracking algorithms (Barbosa Roa et al., 2019). This underscores
48 the critical importance of an anomaly detection method’s ability to adapt to
49 evolving data structures, especially in long-term deployments. Nevertheless,
50 as (Tartakovsky et al., 2013) remarked, immediate detection is not a feasible
51 option unless there is a high tolerance for false alarms.

52 The adaptation of batch models at scale introduces a significant latency in
53 detector adaptation (Wu et al., 2021). Incremental learning methods allowed
54 adaptation while restraining the storage of the whole dataset. The super-
55 vised operator-in-the-loop solution offered by Pannu et al. (2012) showed
56 the detector’s adaptation to data labeled on the flight. Others approached
57 the problem as sequential processing of bounded data buffers in univariate
58 signals (Ahmad et al., 2017) and multivariate systems (Bosman et al., 2015).

59 1.1. Related Work

60 Recent advances in anomaly detection have broadened its scope to include
61 root cause identification governed by the development of explanatory meth-
62 ods capable of diagnosing and tracking faults across the system. Studies can
63 be split into two groups of distinct approaches. The first group approaches
64 explainability as the importance of individual features (Carletti et al., 2019;
65 Nguyen et al., 2019; Amarasinghe et al., 2018). Those studies allow an expla-
66 nation of novelty by considering features independently. The second group
67 uses statistical learning creating models explainable via probability. For in-
68 stance, the integration of variational Bayesian inference probabilistic graph
69 neural network allowed Zhang et al. to model the posterior distribution
70 of sensor dependency for gas leakage localization on unlabeled data (Zhang
71 et al., 2023). Yang et al. recently proposed a Bayesian network (BN) for fault

72 detection and diagnosis. In this BN, individual nodes of the network represent
73 normally distributed variables, whereas the multiple regression model defines weights and relationships. Using the predefined structure of the BN,
74 the authors propose offline training with online detection and diagnosis (Yang et al., 2022).

75 Given the infrequent occurrence of anomalies and their potential absence in training data, the incorporation of synthetic data or feature extraction for various detected events emerges to assist diagnosis of the system. Brito et al. designed synthetic faults based on expert knowledge and introduced them into a transfer learning classifier to exploit faults in rotating machinery, with a subsequent explanation layer (Brito et al., 2023). Conversely, We et al. leveraged feature selection to expose various types of abnormal behavior. The team presents competitive performance while using change in relationships to provide causal inference (Wu et al., 2024).

76 However, it is crucial to underscore that offline training, as previously emphasized, is inherently inadequate when it comes to adapting to anticipated novel patterns, rendering it unsuitable for sustained, long-term operation on IoT devices.

77 This paper emphasizes the importance of combining adaptability in interpretable anomaly detection and proposes a method that addresses this challenge in real industrial systems. Here we report the discovery and characterization of an adaptive anomaly detection method for existing supervisory control and data acquisition (SCADA) systems, employing streaming IoT data. The ability to diagnose multivariate data while providing root cause isolation via statistical learning, extends our previous contribution to the field as presented in (Wadinger and Kvasnica, 2023). The proposed algorithm represents a general method that aids a range of existing safety-critical systems where anomaly diagnosis and identification are paramount.

78 *1.2. Novelty of proposed approach*

79 The idea of using statistical outlier detection is well-established. We highlight the impactful contributions of Yamanishi et al. in (Yamanishi and Takeuchi, 2002; Yamanishi et al., 2004). The authors propose a method for detecting anomalies in a time series. The method is based on the assumption that the continuous data is generated by a mixture of Gaussian distributions, while discrete data is modeled as histogram density. The authors solve the problem of change point detection as well. However, the adaptation system is unaware of such changes, making the moving window the only source

of adaptation. Our self-supervised approach facilitates intelligent adaptation concerning detected change points, to increase the speed of adaptation where the probability of concept drift is high. By leveraging its ability to adapt to changes in operational states, our proposed method operates autonomously when such changes occur. Moreover, Yamanishi et al. (2004) does not attempt to isolate the root cause of the anomaly. Our approach extends statistical outlier detection by incorporating interpretability. This is achieved by evaluating the inverse cumulative distribution function of the latest conditional probabilities for each measurement, considering the remainder of the measurements, and establishing limits that define the threshold for normal event probabilities.

A limited number of studies have focused on adaptation and interpretability within the framework of anomaly detection. Two recent contributions in this area are made by Steenwinckel et al. as reported in (Steenwinckel, 2018; Steenwinckel et al., 2021). In Steenwinckel (2018), the authors emphasize the importance of combining prior knowledge with a data-driven approach to achieve interpretability, particularly concerning root cause isolation. They propose a novel approach that involves extracting features based on knowledge graph pattern extraction and integrating them into the anomaly detection mechanism. This graph is subsequently transformed into a matrix, and adaptive region-of-interest extraction is performed using reinforcement learning techniques. To enhance interpretability, a Generative Adversarial Network (GAN) reconstructs a new graphical representation based on selected vectors. However, it is important to note that the validation of this idealized approach is pending further investigation. Lately, Steenwinckel et al. (2021) introduced a comprehensive framework for adaptive anomaly detection and root cause analysis in data streams. While the adaptation process is driven by user feedback, the specific mechanism remains undisclosed. The authors present an interpretation of their method through a user dashboard, featuring visualizations of raw data. This dashboard is capable of distinguishing between track-related problems and train-related issues, based on whether multiple trains at the same geographical location approach the anomaly. Meanwhile, our efforts are directed towards the development of a self-supervised method that can learn autonomously, reducing the reliance on human supervision, which is often constrained by time limitations and can lead to significant delays in adaptation. Our method is distinguished by its straightforward statistical reasoning and the ability to isolate the root cause of anomalies. The interpretability of our method is demonstrated through

147 the establishment of dynamic operating limits for each signal, leveraging con-
148 ditional probabilities derived from the signal and other system measurements
149 and features. This provides operators with a clear understanding of the sys-
150 tem’s state and the underlying causes of anomalies and offers interoperability
151 with existing alarm handling mechanisms in SCADA which utilize operating
152 limits. To the best of our knowledge, this study appears to be one of the ini-
153 tial attempts to introduce a self-supervised approach for adaptive anomaly
154 detection and root cause isolation in SCADA-based systems utilizing IoT
155 data streams.

156 *1.3. Validation*

157 Two real-world industrial-scale case studies showcase that our proposed
158 method has the capacity to explain anomalies, isolate the root cause, and
159 allow adaptation to change points, allowing long-term deployment at the
160 end users of energy storage systems. We observe similar detection perfor-
161 mance, albeit with lower scalability, on benchmark data when comparing
162 our approach to well-established unsupervised anomaly detection methods
163 in streamed data which create a bedrock for many state-of-the-art contribu-
164 tions, such as One-Class SVM (Amer et al., 2013; Liu et al., 2014; Krawczyk
165 and Woźniak, 2015; Miao et al., 2019; Gözüaçık and Can, 2021), and Half-
166 Space Trees (Wetzig et al., 2019; Lyu et al., 2020).

167 *1.4. Broader Impact*

168 Potential applications of the proposed method are in the field of energy
169 storage systems, where the ability to detect anomalies and isolate their root
170 causes while adapting to changes in operation and environment, is crucial
171 for the system safety. The proposed method is designed to be integrated
172 into the existing infrastructure of the systems, utilizing IoT data streams on
173 top of well-established SCADA systems. SCADA systems continuously mon-
174 itor these process data in real-time, embodying alarm handling mechanisms,
175 which are designed to notify operators of the system’s abnormal behavior
176 and drive attention to the root of the problem. By comparing the current
177 values to the upper and lower operating limits, they take action when a
178 variable exceeds or falls below these limits. However, safe operating limits
179 are often established based on a combination of equipment design limits and
180 the dynamics of the process (Stauffer and Chastain-Knight, 2021). Those
181 are indifferent to the actual state of the system and environmental condi-
182 tions. The proposed method allows the establishment of dynamic operating

183 limits, based on the current state of the system and its environment, with
184 direct utilization in SCADA systems expecting minimal intervention to existing
185 infrastructure. This allows the system to operate closer or further from
186 its design limits, increasing its safety and profitability. The dynamic op-
187 erating limits allow operational metrics monitoring, making potential early
188 detection and prevention easier. Using general adaptable methods without
189 interpretability, on the other hand, may pose safety risks and lower total
190 financial benefits, as the triggered false alarms may need to be thoroughly
191 analyzed, resulting in prolonged downtimes.

192 The main contribution of the proposed solution to the developed body of
193 research is that it:

- 194 • Enriches interpretable anomaly detection with adaptive capabilities
- 195 • Isolates root cause of anomalies while considering interactions
- 196 • Uses self-learning approach on streamed IoT data
- 197 • Demonstrates interpretability by providing operating limits for signals
- 198 • Interoperable with existing SCADA architecture

199 *1.5. Paper Organization*

200 The rest of the paper is structured as follows: We begin with the problem
201 and motivation in **Section 1**, providing context. Next, in **Section 2**, we
202 lay the theoretical groundwork. Our proposed adaptive anomaly detection
203 method is detailed in **Section 3**. We then demonstrate real-world industrial-
204 scale applications in **Section 4**. Finally, we conclude the paper in **Section 5**,
205 summarizing findings and discussing future research directions.

206 **2. Preliminaries**

207 In this section, we present the fundamental ideas that form the basis
208 of the developed approach. Subsection 2.1 explains Welford’s online algo-
209 rithm, which can adjust distribution to changes in real-time. Subsection 2.2
210 proposes a two-pass implementation that can reverse the impact of expired
211 samples. The math behind distribution modeling in Subsection 2.3 estab-
212 lishes the foundation for the Gaussian anomaly detection model discussed in
213 Subsection 2.5, followed by conditional probability computation in Subsec-
214 tion 2.4. The last subsection of the preliminaries is devoted to the definition
215 of anomalies.

216 2.1. Welford's Online Algorithm

217 Welford introduced a numerically stable online algorithm for calculating
 218 mean and variance in a single pass through data. Therefore, the algorithm
 219 allows the processing of IoT device measurements without the need to store
 220 their values (Welford, 1962).

221 Given measurement x_i where $i = 1, \dots, n$ is a sample index in sample
 222 population n , the corrected sum of squares S_n is defined as

$$S_n = \sum_{i=1}^n (x_i - \bar{x}_n)^2, \quad (1)$$

223 with the running mean \bar{x}_n defined as previous mean \bar{x}_{n-1} weighted by pro-
 224 portion of previously seen population $n - 1$ corrected by current sample as

$$\bar{x}_n = \frac{n-1}{n} \bar{x}_{n-1} + \frac{1}{n} x_n = \bar{x}_{n-1} + \frac{x_n - \bar{x}_{n-1}}{n}. \quad (2)$$

225 Throughout this paper, we consider the following formulation of an update
 226 to the corrected sum of squares:

$$S_n = S_{n-1} + (x_n - \bar{x}_{n-1})(x_n - \bar{x}_n), \quad (3)$$

227 as it is less prone to numerical instability due to catastrophic cancellation,
 228 significant loss of precision due to subtracting two nearly equal numbers.

229 Finally, the corresponding unbiased variance is

$$s_n^2 = \frac{S_n}{n-1}. \quad (4)$$

230 This implementation of the Welford method requires the storage of three
 231 scalars: \bar{x}_{n-1} ; n ; S_n .

232 2.2. Inverting Welford's Algorithm

233 Based on (2), it is clear that the influence of the latest sample over the
 234 running mean decreases as the population n grows. For this reason, regulat-
 235 ing the number of samples used for sample mean and variance computa-
 236 tion has crucial importance over adaptation. Given access to the instances used
 237 for computation and expiration period $t_e \in \mathbb{N}_0^{n-1}$, reverting the impact of
 238 x_{n-t_e} can be written as follows

$$S_{n-1} = S_n - (x_{n-t_e} - \bar{x}_{n-1})(x_{n-t_e} - \bar{x}_n), \quad (5)$$

239 where the reverted mean is given as

$$\bar{x}_{n-1} = \frac{n}{n-1}\bar{x}_n - \frac{1}{n-1}x_{n-t_e} = \bar{x}_n - \frac{x_{n-t_e} - \bar{x}_n}{n-1}. \quad (6)$$

240 Finally, the unbiased variance follows the formula:

$$s_{n-1}^2 = \frac{S_{n-1}}{n-2}. \quad (7)$$

241 Notably, inversion allows the algorithm to keep a constant rate of adap-
242 tation at the cost of storing a bounded data buffer.

243 2.3. Statistical Model of Multivariate System

244 Multivariate normal distribution generalizes the multivariate systems to
245 the model where the degree to which variables are related is represented by
246 the covariance matrix. Gaussian normal distribution of variables is a reason-
247 able assumption for process measurements, as it is a common distribution
248 that arises from stable physical processes measured with noise (Mishra and
249 Datta-Gupta, 2018). The general notation of multivariate normal distribu-
250 tion is:

$$\mathbf{X} \sim \mathcal{N}_k(\boldsymbol{\mu}, \boldsymbol{\Sigma}), \quad (8)$$

251 where k -dimensional mean vector is denoted as $\boldsymbol{\mu} = (\bar{x}_1, \dots, \bar{x}_k)^T \in \mathbb{R}^k$
252 and $\boldsymbol{\Sigma} \in \mathbb{R}^{k \times k}$ is the $k \times k$ covariance matrix, where k is the index of last
253 random variable.

254 The probability density function (PDF) $f(\mathbf{x}; \boldsymbol{\mu}, \boldsymbol{\Sigma})$ of multivariate normal
255 distribution is denoted as:

$$f(\mathbf{x}; \boldsymbol{\mu}, \boldsymbol{\Sigma}) = \frac{1}{(2\pi)^{k/2} |\boldsymbol{\Sigma}|^{1/2}} e^{-\frac{1}{2}(\mathbf{x}-\boldsymbol{\mu})^\top \boldsymbol{\Sigma}^{-1}(\mathbf{x}-\boldsymbol{\mu})}, \quad (9)$$

256 where \mathbf{x} is a k -dimensional vector of measurements x_i at time i , $|\boldsymbol{\Sigma}|$
257 denotes the determinant of $\boldsymbol{\Sigma}$, and $\boldsymbol{\Sigma}^{-1}$ is the inverse of $\boldsymbol{\Sigma}$.

258 The cumulative distribution function (CDF) of a multivariate Gaussian
259 distribution describes the probability that all components of the random
260 vector \mathbf{X} take on a value less than or equal to a particular point q in space,
261 and can be used to evaluate the likelihood of observing a particular set of
262 measurements or data points. In other words, it gives the probability of

263 observing a random vector that falls within a certain region of space. The
264 standard notation of CDF is as follows:

$$F(\mathbf{x}; \boldsymbol{\mu}, \boldsymbol{\Sigma}) = \int_{-\infty}^q f(\mathbf{x}; \boldsymbol{\mu}, \boldsymbol{\Sigma}) d\mathbf{x}, \quad (10)$$

265 where $d\mathbf{x}$ denotes the integration over all k dimensions of \mathbf{x} .

266 As the equation (10) cannot be integrated explicitly, an algorithm for
267 numerical computation was proposed in Genz (2000).

268 Given the PDF, we can also determine the value of \mathbf{x} that corresponds to a
269 given quantile q using a numerical method for inversion of CDF (ICDF) often
270 denoted as percent point function (PPF) or $F(\mathbf{x}; \boldsymbol{\mu}, \boldsymbol{\Sigma})^{-1}$. An algorithm that
271 calculates the value of the PPF is part of standard statistical software tools.

272 2.4. Conditional Probability Distribution

273 Considering that we observe particular vector \mathbf{x}_i , we can update probabil-
274 ity distributions, calculated according to the rules of conditional probability,
275 of individual measurements within the vector given the rest of the measure-
276 ments in \mathbf{x}_i . Let's assume multivariate normal distribution (8) and without
277 loss of generality, that the vector \mathbf{x}_i can be partitioned into subset variable
278 x_a , and complement vector \mathbf{x}_b as follows

$$\mathbf{x}_i = \begin{bmatrix} x_a \\ \mathbf{x}_b \end{bmatrix} \text{ with dimensions } \begin{bmatrix} 1 \times 1 \\ (k-1) \times 1 \end{bmatrix}, \quad (11)$$

279 where $a = 1, \dots, k$ and $\mathbf{b} = \{1, 2, \dots, k\}$ where $a \notin \mathbf{b}$. This partitioning
280 allows us to define block-wise mean and covariance as follows:

$$\boldsymbol{\mu} = \begin{bmatrix} \mu_a \\ \boldsymbol{\mu}_b \end{bmatrix} \text{ with dimensions } \begin{bmatrix} 1 \times 1 \\ (k-1) \times 1 \end{bmatrix}, \quad (12)$$

281 and

$$\boldsymbol{\Sigma} = \begin{bmatrix} \sigma_{aa}^2 & \boldsymbol{\Sigma}_{ab} \\ \boldsymbol{\Sigma}_{ba} & \boldsymbol{\Sigma}_{bb} \end{bmatrix} \text{ with dimensions } \begin{bmatrix} 1 \times 1 & 1 \times (k-1) \\ (k-1) \times 1 & (k-1) \times (k-1) \end{bmatrix}. \quad (13)$$

282 Subsequently, we can derive the conditional distribution of any subset
283 variable x_a , given the complementary vector \mathbf{x}_b . This conditional distribution
284 conforms to a univariate normal distribution, characterized by:

$$X_a | \mathbf{X}_b \sim \mathcal{N}(\mu_{a|\mathbf{b}}, \sigma_{a|\mathbf{b}}^2). \quad (14)$$

285 where $\mu_{a|b}$ denotes the conditional mean and $\sigma_{a|b}^2$ represents the conditional variance. These crucial parameters can be computed by applying the
 286 Schur complement as follows:
 287

$$\sigma_{a|b}^2 = \sigma_{aa}^2 - \Sigma_{ab}\Sigma_{bb}^{-1}\Sigma_{ba}, \quad (15)$$

288 for the conditional variance $\sigma_{a|b}^2$, while the conditional mean, denoted as
 289 $\mu_{a|b}$, is determined by:

$$\mu_{a|b} = \mu_a + \Sigma_{ab}\Sigma_{bb}^{-1}(\mathbf{x}_b - \boldsymbol{\mu}_b). \quad (16)$$

290 The conditional variance $\sigma_{a|b}^2$ essentially represents the Schur complement
 291 of Σ_{bb} within the overall covariance matrix Σ .

292 2.5. Gaussian Anomaly Detection

293 From a viewpoint of statistics, outliers are commonly denoted as values
 294 that significantly deviate from the mean. Under the assumption that the
 295 spatial and temporal characteristics of a system, observed over a moving
 296 window, can be suitably represented as normally distributed features, we
 297 assert that any anomaly can be identified as an outlier.

298 In empirical fields like machine learning, the three-sigma rule (3σ) provides
 299 a framework for characterizing the region of a distribution within which
 300 normal values are expected to fall with high confidence. This rule renders
 301 approximately 0.265% of values in the distribution as anomalous.

302 The 3σ rule establishes the probability that any sample x_a of a random
 303 vector X falls within a given CDF over a semi-closed interval as the distance
 304 from the conditional mean $\mu_{a|b}$ of 3 conditional variances $\sigma_{a|b}^2$ and gives an
 305 approximate value of q as

$$q = P\{|x_a - \mu_{a|b}| < 3\sigma_{a|b}^2\} = 0.99735. \quad (17)$$

306 Utilizing a probabilistic model of normal behavior, we can determine
 307 threshold values x_l and x_u corresponding to the closed interval of the CDF
 308 where this probability is established. The inversion of Equation (10) facilitates
 309 this calculation, yielding:

$$x_l = F((1 - P\{|x_a - \mu_{a|b}| < 3\sigma_{a|b}^2\}); \mu_{a|b}, \sigma_{a|b}^2)^{-1}, \quad (18)$$

310 for the lower limit, and

$$x_u = F((P\{|x_a - \mu_{a|\mathbf{b}}| < 3\sigma_{a|\mathbf{b}}^2\}); \mu_{a|\mathbf{b}}, \sigma_{a|\mathbf{b}}^2)^{-1}, \quad (19)$$

311 for the upper limit. These lower and upper limits together form vectors
 312 \mathbf{x}_l and \mathbf{x}_u , respectively, defining the region of normal system operation. This
 313 region is conceptualized as a hypercube in the feature space, with each di-
 314 mension bounded by the corresponding feature limits, as computed using
 315 Equations (18) and (19) for all $a = 1, \dots, k$; $\mathbf{b} = \{1, 2, \dots, k\}$ where $a \notin \mathbf{b}$.
 316 The approximation of a confidence ellipse as a hypercube can be employed
 317 to represent the region of normal system operation for individual variables
 318 of a multivariate system, rendering it as an aid for visual representation.

319 The predicted state of the system, denoted as y_i , and the normality of
 320 signals $\mathbf{y}_{s,i}$ at time i are determined based on the maximum distance of
 321 observations from the center of the probabilistic density. The center of the
 322 probabilistic density corresponds to the vector of conditional means $\mu_{a|\mathbf{b}}$ with
 323 respect to other features. The calculation of this distance involves the cumu-
 324 lative distribution function (CDF) of observations and conditional distribu-
 325 tions, as follows:

$$F(x_a; \mu_{a|\mathbf{b}}, \sigma_{a|\mathbf{b}}^2) : a = 1, \dots, k; \mathbf{b} = \{1, 2, \dots, k\} \text{ where } a \notin \mathbf{b}. \quad (20)$$

326 Subsequently, operation states of individual inputs are defined as follows:

$$\mathbf{y}_{s,i} = \begin{cases} 0 & \text{if } T \leq (20) \\ 1 & \text{if } T > (20), \end{cases} \quad (21)$$

327 where T represents a threshold that distinguishes between normal signal
 328 measurement ($\mathbf{y}_{s,i} = 0$) and abnormal ($\mathbf{y}_{s,i} = 1$).

329 For the overall abnormality of the system, any anomaly in signals $\mathbf{y}_{s,i}$ is
 330 considered, resulting in:

$$y_i = \begin{cases} 1 & \text{if } 1 \in \mathbf{y}_{s,i} \\ 0 & \text{otherwise,} \end{cases} \quad (22)$$

331 defining the discrimination boundary between system operation where
 332 $y_i = 0$ indicates normal system operation, and $y_i = 1$ indicates anomalous
 333 operation.

334 *2.6. Anomaly Definition*

335 This subsection provides an overview of the definition of anomalies in
336 data analysis and their categorization, setting conventions for this paper.

337 In the realm of data analysis, anomalies are conspicuous deviations from
338 the anticipated patterns within a dataset. Traditionally, the task of anomaly
339 detection has relied upon unsupervised methodologies, wherein the identifi-
340 cation of "outliers" entails the comparison of data points in both temporal
341 and spatial contexts. This approach, often referred to as point-wise anomaly
342 detection, classifies a data point as an anomaly when it exhibits significant
343 dissimilarity from its neighboring data points (Iglesias Vázquez et al., 2023).

344 The concept of point anomalies, influenced by factors such as temporal
345 and spatial aspects, can be further categorized into conditional and contex-
346 tual anomalies (Ruff et al., 2021).

347 Nevertheless, this conventional method may not be suitable for scenarios
348 characterized by collective anomalies, where clusters of abnormal data points
349 coexist. A more pragmatic approach defines anomalies as deviations from
350 established "normal" patterns, resembling the principles of semi-supervised
351 learning. Change point detection, in a similar vein, can be regarded as a
352 relative approach that takes into account the varying dynamics of changes,
353 whether they occur gradually or abruptly (Iglesias Vázquez et al., 2023).

354 It is imperative to recognize that the interpretation of anomalies, outliers,
355 and novelties can vary upon the application. Anomalies typically garner
356 significant attention, while outliers are often treated as undesirable noise
357 and are typically excluded during data preprocessing. Novelties, on the other
358 hand, signify new observations that necessitate model updates to adapt to
359 an evolving environment (Ruff et al., 2021).

360 Notwithstanding the differences in terminology, methods employed for the
361 identification of data points residing in low-probability regions, irrespective of
362 whether they are referred to as "anomaly detection," "outlier detection," or
363 "novelty detection," share fundamental similarities (Iglesias Vázquez et al.,
364 2023).

365 **3. Adaptive Anomaly Detection and Interpretation Framework**

366 In this section, we propose an adaptive and interpretable detection frame-
367 work (AID) for multivariate systems with streaming IoT devices. This ap-
368 proach models the system as a dynamic joint normal distribution, enabling
369 it to effectively adapt to pervasive nonstationary effects on processes. Our

370 method handles various factors, including change points, concept drift, and
371 seasonal effects. Our primary contribution lies in the fusion of an adaptable
372 self-supervised system with root cause identification capabilities. This combi-
373 nation empowers the online statistical model to diagnose anomalies through
374 two distinct mechanisms. Firstly, it employs conditional probability calcu-
375 lations to assess the system’s operating conditions’ normality. Secondly, it
376 identifies outliers within individual signal measurements and features based
377 on dynamic alert-triggering operating limits. In the following sections, we
378 describe our proposed methodology across three subsections. The initial sub-
379 section delves into the process of initializing the model’s parameters. The
380 subsequent section describes online training and adaptation, while the final
381 subsection expounds upon the model’s detection and diagnostic capabilities.
382 For a concise representation of the proposed method, Algorithm 1 is provided.

383 *3.1. Model Parameters Initialization*

384 The model initialization is governed by defining two tunable hyperparam-
385 eters of the model: the expiration period (t_e) and the threshold (T). The
386 expiration period determines the window size for time-rolling computations,
387 impacting the proportion of outliers within a given timeframe, and directly
388 influencing the relaxation (with a longer expiration period) or tightening
389 (with a shorter expiration period) of dynamic signal limits. Additionally, we
390 introduce a grace period, which defaults to $3/4t_e$, allowing for model calibra-
391 tion. During this grace period, system anomalies are not flagged to prevent
392 false positives and speed up self-supervised learning, introduced in Subsec-
393 tion 3.2. The length of the expiration period inversely correlates with the
394 model’s ability to adapt to sudden changes. The adaptation and detection
395 of shifts in the data-generating process, such as changes in mean or variance,
396 is managed through the adaptation period t_a . A longer t_a results in slower
397 adaptation but potentially longer alerts, which can be valuable when collec-
398 tive anomalies are expected to occur. In most cases, $t_a = t_e$ offers optimal
399 performance.

400 As a general rule of thumb, expiration period t_e should be determined
401 based on the slowest observed dynamics within the multivariate system. The
402 threshold T defaults to the three-sigma probability of q in (17). Adjusting
403 this threshold can fine-tune the trade-off between precision and recall. A
404 lower threshold boosts recall but may lower precision, while a higher thresh-
405 old enhances precision at the cost of recall. The presence of one non-default

406 easily interpretable hyperparameter facilitates adaptability to various sce-
407 narios. We recommend starting with the default values of other parameters
408 and making adjustments based on real-time model performance.

409 *3.2. Online training*

410 AID training follows an incremental learning approach, processing each
411 new sample upon arrival. Incremental learning allows online parameter up-
412 dates, albeit with a potential computational delay affecting response latency.

413 In the case of a dynamic joint probability distribution, the parameters are
414 μ_i and Σ_i at time instance i . Update of the mean vector μ_i and covariance
415 matrix Σ_i is governed by Welford's online algorithm using equation (2) and
416 (4) respectively. Samples beyond the expiration period t_e are disregarded
417 during the second pass. The effect of expired samples is reverted using inverse
418 Welford's algorithm for mean (6) and variance (7), accessing the data in the
419 buffer. For details, refer to Subsection 2.2.

420 It is worth noting that adaptation relies on two self-supervised methods.
421 Adaptation routine runs if the observation at time instance i is considered
422 normal. Furthermore, adaptation period t_a allows the model to update the
423 distribution on collective anomalies as well, thus speeding up the adaptation
424 to change points. Given the predicted system anomaly state from (22) as y_i
425 over the window of past observations $\mathbf{y}_i = \{y_{i-t_a}, \dots, y_i\}$, the following test
426 holds when adaptation is performed on outlier:

$$\frac{\sum_{y \in \mathbf{y}_i} y}{n(\mathbf{y}_i)} > T. \quad (23)$$

427 Here $n(\mathbf{y}_i)$ denotes the dimensionality of \mathbf{y}_i . The logic of the (23) follows
428 that over an adaptation period t_a , the changepoint can be discriminated from
429 collective anomalies and point anomalies by their minimum duration, while
430 T allows some overlap with previous normal conditions.

431 *3.3. Online prediction*

432 In the prediction phase, multiple metrics are evaluated to assess the state
433 of the modeled system.

434 Firstly, we calculate the parameters of the conditional distribution con-
435 cerning the dynamic multivariate Gaussian distribution. These calculations

436 are performed for the process observation vector \mathbf{x}_i at time instance i . Specifically,
437 we compute the conditional mean using (16) and the conditional variance
438 using (15). These computations yield univariate conditional distributions
439 for individual signals and features. These conditional distributions play
440 a crucial role in assessing the abnormality of signals and features concerning
441 other observed values. This assessment relies on the strength of relationships
442 defined by the covariance matrix of the dynamic multivariate Gaussian
443 distribution. Consequently, our approach inherently considers the interactions
444 between input signals and features. The determination of anomalous
445 behavior is governed by (21).

446 Any anomaly detected within one of the features triggers an alert at the
447 system level. The decision regarding the overall system's anomalous behavior
448 is guided by (22). Nevertheless, individual determinations of anomalies serve
449 as a diagnostic tool for isolating the root cause of anomalies.

450 To assist operators in their assessments, we establish a hypercube de-
451 fined by lower and upper threshold values, denoted as \mathbf{x}_l and \mathbf{x}_u , respec-
452 tively. These thresholds are derived from (18) and (19), incorporating up-
453 dated model parameters. Lower and upper thresholds play a pivotal role
454 as dynamic operating limits. They replace the conservative operating lim-
455 its provided in sensor documentation, accounting for spatial factors, such as
456 multipoint measurements, temporal factors such as aging, and actual envi-
457 ronmental conditions that influence sensor operation.

458 Our framework anticipates unexpected novel behavior, including signal
459 loss. This anticipation involves calculating the cumulative distribution func-
460 tion (CDF) over the univariate normal distribution of sampling, focusing
461 on the differences between subsequent timestamps. We operate under the
462 assumption that, over the long term, the distribution of sampling times re-
463 mains stable. As a result, we employ a one-pass update mechanism utilizing
464 (2) and (4), for efficiency. To proactively detect subtle changes in sampling
465 patterns, self-supervised learning is employed, leveraging anomalies weighted
466 by the deviation from $(1 - F(x_i; \mu, \sigma^2))$ for training.

467 The system is vigilant in identifying change points. When the adaptation
468 test specified in (23) is satisfied, change points are flagged and isolated.
469 This initiation of change points triggers updates to the model, as stated in
470 Subsection 3.2. ensuring it adapts to evolving data patterns, such as changes
471 in operation state, effectively.

Algorithm 1 Online Detection and Identification Workflow

Input: expiration period t_e

Output: system anomaly y_i , signal anomalies $\mathbf{y}_{s,i}$, sampling anomaly $y_{t,i}$, change-point $y_{c,i}$, lower thresholds $\mathbf{x}_{l,i}$, upper thresholds $\mathbf{x}_{u,i}$,

Initialisation :

- 1: $i \leftarrow 1; n \leftarrow 1; T \leftarrow (17); \boldsymbol{\mu} \leftarrow \mathbf{x}_0; \boldsymbol{\Sigma} \leftarrow \mathbf{1}_{k \times k}; \mu_t \leftarrow 0; \sigma_t^2 \leftarrow 1;$
 - 2: compute $F(\mathbf{x}_0; \boldsymbol{\mu}, \boldsymbol{\Sigma})$ using algorithm in Genz (2000);
LOOP Process
 - 3: **loop**
 - 4: $\mathbf{x}_i, t_i \leftarrow \text{RECEIVE}();$
 - 5: $\mathbf{y}_{s,i} \leftarrow \text{PREDICT}(\mathbf{x}_i, T)$ using (21);
 - 6: $y_i \leftarrow \text{PREDICT}(\mathbf{y}_{s,i})$ using (22);
 - 7: $\mathbf{x}_{l,i}, \mathbf{x}_{u,i} \leftarrow \text{GET}(T, \boldsymbol{\mu}, \boldsymbol{\Sigma})$ using (18), (19);
 - 8: $y_{t,i} \leftarrow \text{PREDICT}(t_i - t_{i-1})$ using (21);
 - 9: $\mu_t, \sigma_t^2 \leftarrow \text{UPDATE}(t_i - t_{i-1}, \mu_t, \sigma_t^2)$ using (2), (4);
 - 10: **if** (22) = 0 **or** (23) **then**
 - 11: $\boldsymbol{\mu}, \boldsymbol{\Sigma} \leftarrow \text{UPDATE}(\mathbf{x}_i, \boldsymbol{\mu}, \boldsymbol{\Sigma}, n)$ using (2), (4);
 - 12: **if** (23) **then**
 - 13: $y_{c,i} \leftarrow 1;$
 - 14: **else**
 - 15: $y_{c,i} \leftarrow 0;$
 - 16: **end if**
 - 17: $n \leftarrow n + 1;$
 - 18: **for** \mathbf{x}_{i-t_e} **do**
 - 19: $\boldsymbol{\mu}, \boldsymbol{\Sigma} \leftarrow \text{REVERT}(\mathbf{x}_{i-t_e}, \boldsymbol{\mu}, \boldsymbol{\Sigma}, n)$ using (6), (7);
 - 20: $n \leftarrow n - 1;$
 - 21: **end for**
 - 22: **end if**
 - 23: $i \leftarrow i + 1;$
 - 24: **end loop**
-

⁴⁷² **4. Case Study**

⁴⁷³ This section presents two case studies on real industrial-scale energy stor-
⁴⁷⁴ ages and a real data benchmark to demonstrate the effectiveness and appli-
⁴⁷⁵ability of our proposed approach. We investigate the properties and per-
⁴⁷⁶formance of the approach using signals from IoT devices in an energy system

477 and streamed benchmark system data. The successful deployment demon-
478 strates that this approach is suitable for existing industrial systems utilizing
479 IoT data streams on top of well-established SCADA systems.

480 *4.1. Battery Energy Storage System TERRA*

481 In the first case study, we demonstrate our proposed method on real
482 industrial-scale battery energy storage system (BESS) TERRA, depicted in
483 Fig 1. TERRA has an installed capacity of 151 kWh distributed among
484 10 modules with 20 cells. The Inverter's nominal power is 100 kW. The
485 TERRA reports measurements of State of Charge (SoC), supply/draw energy
486 set-points, and inner temperature, at 6 positions (channels) of each battery
487 module. A substantial size of the system, which is 2.4x2.4x1.2m (HxWxD),
488 requires a proper cooling mechanism. The cooling is handled by forced air
489 from the HVAC system and inner fans, while the fire safety system is passive.
490 Tight battery temperature control is needed to optimize performance and
491 maximize the safety and battery's lifespan. Identifying anomalous events
492 and removal of corrupted data might yield significant improvement in the
493 process control level and increase the reliability and stability of the system.



Figure 1: Photograph of the actual studied TERRA energy storage unit with open doors (left), and closed doors (right).

494 The AID is integrated into the existing software infrastructure of the
495 system, allowing detection and diagnosis of the system using streamed IoT

496 data. Here we replay a 9-day stream of historical measurements of the device,
497 to demonstrate key features of AID.

498 For demonstration purposes, the expiration period t_e is set to 4 days, as
499 the system is expected to adapt to the new behavior, due to the transfer of
500 the module to the outside. The grace period was reduced to 1 day, to observe
501 the reaction to concept drift. The threshold T is set to 3.5σ to reduce the
502 number of alarms. The frequency will be higher as the detector is protected
503 and self-supervised. The adaptation period t_a is changed to 3 hours as this
504 is the time constant of the temperature to the unit change of supply/draw
505 power demand.

506 Figure 2 depicts the average cell temperature measurement of the TERRA
507 for all 10 modules. The data are normalized to the range [0, 1] to protect
508 the sensitive business value. The light red area represents the region out of
509 dynamic operating limits as provided by AID. On 7th March 2022, the system
510 was relocated from the inside of the building to the outside power socket. The
511 system was expected to adapt to the new behavior within 4 days as specified
512 by t_e . Nevertheless, due to the protection of the model from learning the
513 anomalous data, the new behavior could not be captured as the system was
514 not operating within the safe limits. The adaptation started three days later,
515 as only some of the measurements within the safe region after transfer were
516 learned. Therefore, the importance of self-supervised adaptation to changes
517 in data is crucial. As we can see, the change points detection according to
518 (23) alerted such change shortly after the TERRA was connected to a data
519 broker, while the length of the adaptation period enabled discrimination from
520 collective anomaly.

521 In Figure 3 we depict the same measurement with a changepoint adap-
522 tation mechanism in place. The mechanism speeds up the adaptation to the
523 new behavior, as the system is allowed to learn from anomalous data when
524 they represent the changed behavior. The adaptation took approximately 6
525 times shorter.

526 The default sampling rate of the incoming signal measurements is 1
527 minute. However, network communication of the IoT devices is prone to
528 packet dropout, which results in unexpected non-uniformities in sampling
529 from the perspective of the SCADA system. The transfer of TERRA was
530 accompanied by the disconnection of IoT sensors from the data broker which
531 might be considered an anomaly. The system can detect such anomalies as
532 well, as depicted in Figure 4. Along with known disconnection, the system
533 alerted two more non-uniformities of shorter extend, scaled in the figure for

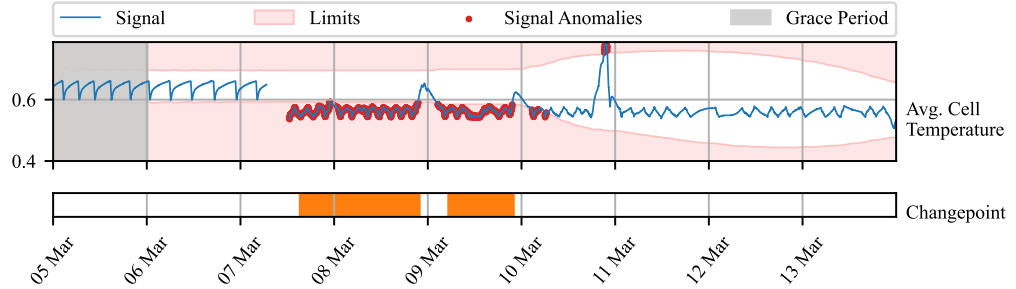


Figure 2: Time series of TERRA measurements observed over 9 days (blue line). The y-axis renders the average temperature of all cells and modules after the normalization to the range of [0, 1]. The light red area represents an area out of dynamic operating limits for individual signals. Observations out of the limits are marked by a red dot. Orange bars represent the times, at which changepoints were detected. Grace period is grayed out.

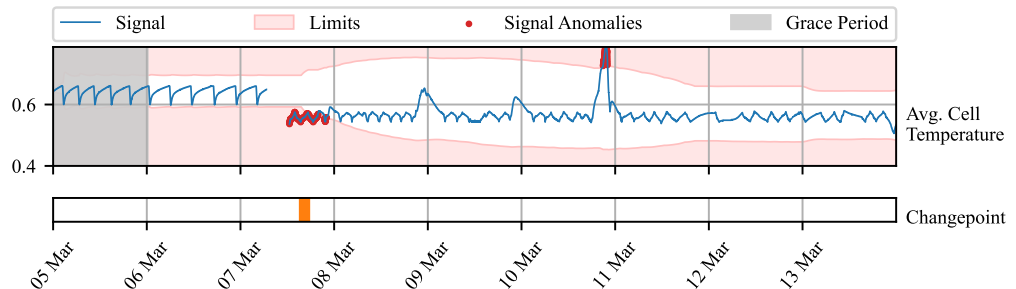


Figure 3: Time series of TERRA measurements observed over 9 days (blue line). The y-axis renders the average temperature of all cells and modules after the normalization to the range of [0, 1]. The light red area represents an area out of dynamic operating limits for individual signals. Observations out of the limits are marked by a red dot. Orange bars represent the times, at which changepoints were detected. Grace period is grayed out.

534 better visibility. The short loss of signal was caused by the packet drop, as
 535 it impacted only a few consecutive measurements. Various confidence levels
 536 could be used to further analyze and map potential causes to the duration
 537 of the outage.

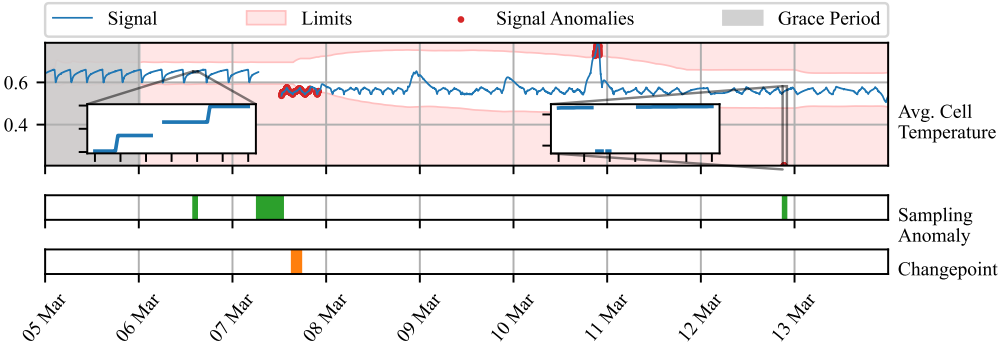


Figure 4: Time series of TERRA measurements observed over 9 days (blue line). The y-axis renders the average temperature of all cells and modules after the normalization to the range of [0, 1]. The light red area represents an area out of dynamic operating limits for individual signals. Observations out of the limits are marked by a red dot. Orange bars represent the times, at which changepoints were detected. Green bars represent periods where sampling anomaly was alerted. Grace period is grayed out.

538 Lastly, we want to acknowledge the outlier, left uncaptured due to in-
 539 creased variance of the distribution in a period of adaptation. Observing
 540 multiple variables, where some might be influenced less by the change in be-
 541 havior, might be beneficial in such cases. The industrial partner provided a
 542 physical model of the battery module temperature, defined as follows:

$$\begin{aligned} T_{\text{bat},i+1} = & T_{\text{bat},i} + T_s(q_{\text{fan}} V_{\text{b,max}} \rho c_p (T_{\text{out}} - T_{\text{bat},i}) + V_{\text{c,max}} q_{\text{circ.fan}} \rho c_p T_{\text{bat},i} \\ & + q_{\text{circ.fan}} (P_{\text{cool}} q_{\text{cool}} P_{\text{heat}} q_{\text{heat}}) + c_{\text{scale}} Q_{\text{bat}} + q_{\text{inner fans}} \\ & - (V_{\text{b,max}} q_{\text{fan}} V_{\text{c,max}} q_{\text{circ.fan}}) \rho c_p T_{\text{bat},i}) / (m_{\text{bat}} c_{\text{p,b}}) \end{aligned} \quad (24)$$

543 When combined with an averaged measurement of battery module tem-
 544 perature, we could compute the difference between real and predicted tem-
 545 perature. Such deviation can be useful in detecting unexpected patterns in
 546 temperature due to the impact of external disturbance and aging. Neverthe-
 547 less, it may be inaccurate as the physical model is simplified and does not
 548 account for spatial aspects, like temperature gradients as well as different

dynamic effects of charging and discharging on temperature. For instance, in Fig. 1 during the first two days we see, that the cooling dynamic is not captured well, resulting in a subtle positive difference between average cell temperature and the temperature predicted by the model. In combination with the raw measured average of the temperature, the AID captures the outlier on 9th March which could not be captured in a univariate setting. The physical model exposes temporal aspects of the behavior as it considers the dynamics of its inputs. The rapid increase in temperature w.r.t the modeled dynamics due to environmental conditions will draw a sharp positive peak in the difference between the real and predicted temperature, which will slowly vanish. Based on the significance of the deviation, the peak will be notified as a single-point anomaly or collective anomaly.

This case study demonstrated AID’s effectiveness within the context of the energy storage system, specifically the TERRA system. The AID system exhibited adaptability to changes in the operational environment, contributing to its versatility and robustness. Additionally, it facilitated the establishment of dynamic operating limits for SCADA systems, considering context of the device such as environmental conditions or aging. Furthermore, the AID system showcased its capability to operate with a physical model, enhancing the precision of anomaly detection processes. This highlights the potential of AID as a valuable tool within complex industrial systems. The validity of our proposed approach was verified by our industrial partner, who confirmed that the detected anomalies were indeed caused by the aforementioned events.

4.2. Kokam Battery Module

A second case study presents temperature profile monitoring of individual modules of battery pack TERRA deployed at the premises of the end user. During the operation, a hardware fault of module’s 9 cooling fan occurred on 23rd August 2023 at 17:12:30. Our industrial partner was interested in finding out, whether such an event could be captured by an anomaly detection system. Each of the 10 modules, embodies 20 cells measured by 6 spatially distributed sensors as shown in Figure 6. The measurements are sent in 30-second intervals and processed in a streamed manner by SCADA. With the availability of the temperature profiles for all the modules, we computed the deviation of the observed value from the average of all the modules’ temperature measurements. The ground truth information about the fan fault was provided to the best of the operator’s knowledge. However, this information serves for evaluation only, as the system operates in a self-supervised manner.

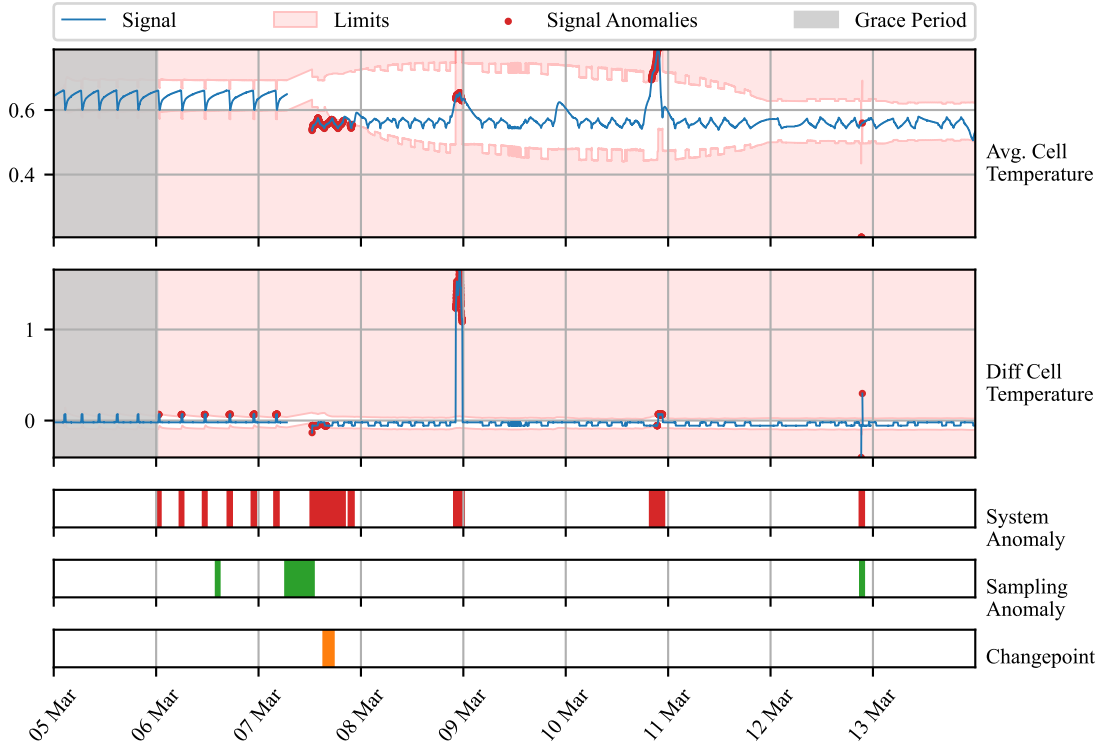


Figure 5: Time series of TERRA measurements observed over 9 days (blue line). The y-axis renders the average temperature of all cells and modules after the normalization to the range of [0, 1]. The light red area represents an area out of dynamic operating limits for individual signals. Observations out of the limits are marked by a red dot. Orange bars represent the times, at which changepoints were detected. Green bars represent periods where sampling anomaly was alerted. Red bars denote the period where any of the signals contained anomaly. Grace period is grayed out.

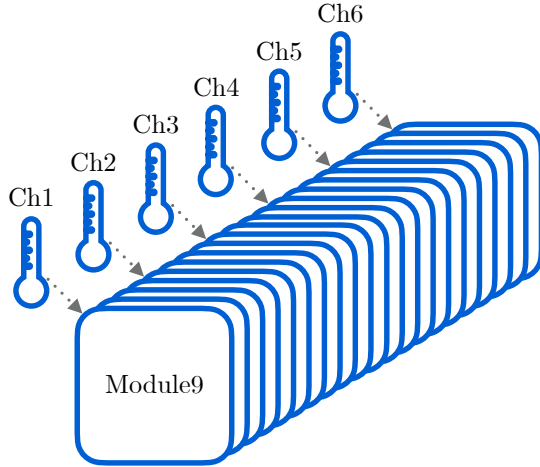


Figure 6: Module 9 with 20 cells and 6 sensors measuring the temperature at each 4th cell.

Our anomaly detection system was, in this case, initialized for the operation in production. The expiration period of 7 days, allowed the system to adapt to weekly seasonality due to the usage of the battery following work week. The grace period was kept at the default value, equal to t_e . The threshold value was shifted to a 4 sigma value of 99.977% which makes the frequency of anomalous events approximately once a week given 30-second sampling. The adaptation period was held constant as the deployed system is not expected to change its behavior dramatically on a daily basis.

In Figure 7 we observe 4 days of operation around the period of fan fault occurrence. The deviations between the observed temperature measured by channels of module 9 and the average temperature of all modules are displayed. The dynamic operating limits tightly envelop temperatures measured by the sensors in the middle of the module (refer to Figure 6), while measurements at both sides deviate more due to the proximity to the walls and sources of disturbance. We observed multiple alarms raised by various channels individually before the fan fault. These anomalies, while not addressed here further, could be subjects of interest for further investigation by system operators. Meanwhile, the fan fault at the center of our focus is alarmed based on three measurements, namely channels 1, 2, and 3. From the zoomed views, we can observe a sharp increase in the temperature devia-

606 tion. The alarm is on until 24th August at noon, when significant fluctuations
607 vanish followed by temporary settling of the temperature. On 25th August
608 at 11:21, increased temperature fluctuations are followed by an increase of
609 temperature similar to the initial one. AID alerts this fault again based on
610 measurements by channels 1, 2, and 3.

611 Time series of TERRA measurements observed over 9 days (blue line).
612 The y-axis renders the average temperature of all cells and modules after the
613 normalization to the range of [0, 1]. The light red area represents an area out
614 of dynamic operating limits for individual signals. Observations out of the
615 limits are marked by a red dot. Orange bars represent the times, at which
616 changepoints were detected. Green bars represent periods where sampling
617 anomaly was alerted. Red bars denote the period where any of the signals
618 contained anomaly. Grace period is grayed out.

619 Interestingly, during the presence of a fault in the fan, two more peri-
620 ods where the fan started operating again followed as depicted in Figure 8.
621 Periods of operation were interrupted again on 27th and 28th August respec-
622 tively in the early morning hours. In both of the cases, AID detected the
623 presence of the fault at the moment of occurrence. In the first case, channel
624 3 reported an anomaly slightly before the increase in temperature, due to
625 abnormal fluctuation happening prior to faults.

626 This case study demonstrates the effectiveness of the AID framework in
627 identifying hardware faults within the context of energy storage systems. It
628 showcases the system’s ability to harness spatially distributed sensors that
629 measure the same process variable. The AID system successfully pinpointed
630 a fault in a cooling fan during real-world production operations, underlining
631 its practical utility and its relevance in enhancing the safety of energy storage
632 systems. Furthermore, the incorporation of adaptation mechanisms ensures
633 that the system can be deployed over extended periods without necessitating
634 resource-intensive retraining. Additionally, the concept of dynamic operating
635 limits introduced in this study holds promise for integration with Supervisory
636 Control and Data Acquisition (SCADA) monitoring systems, enabling proac-
637 tive responses in situations where human life, equipment, or the environment
638 may be at risk.

639 *4.3. Real Data Benchmark*

640 The benchmarking comparison in this subsection evaluates the AID frame-
641 work against adaptive unsupervised detection methods, specifically One-
642 Class Support Vector Machine (OC-SVM) and Half-Space Trees (HS-Trees).

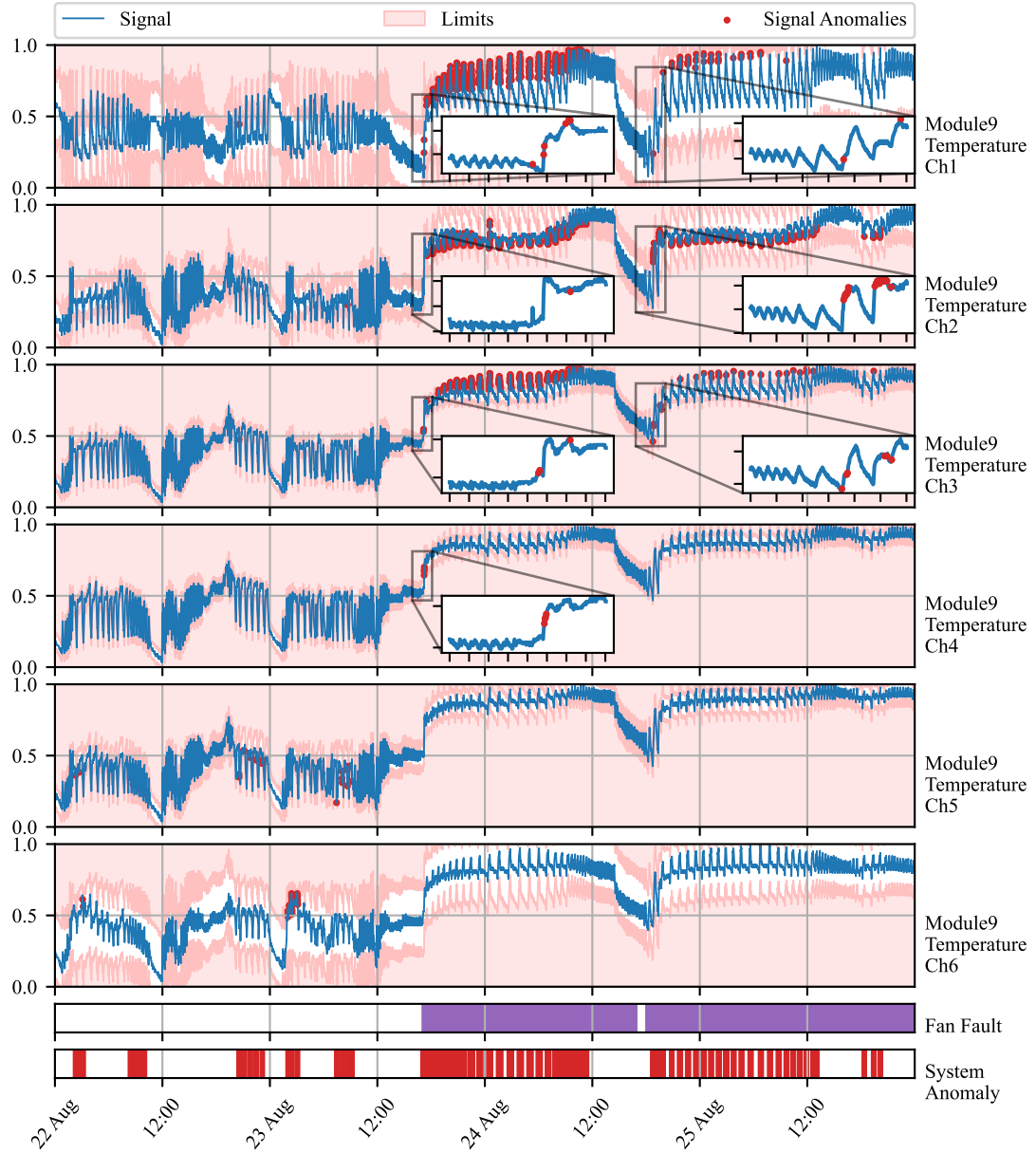


Figure 7: Time series of battery module 9 measurements (blue line). The y-axis renders the normalized deviations of temperature from the average of all modules. Signal anomalies are marked as red dots. The light red area represents an area out of dynamic operating limits. True fan faults are marked by purple bars. Green bars represent the times of changepoint detection. Red bars denote the period where any signal anomaly.

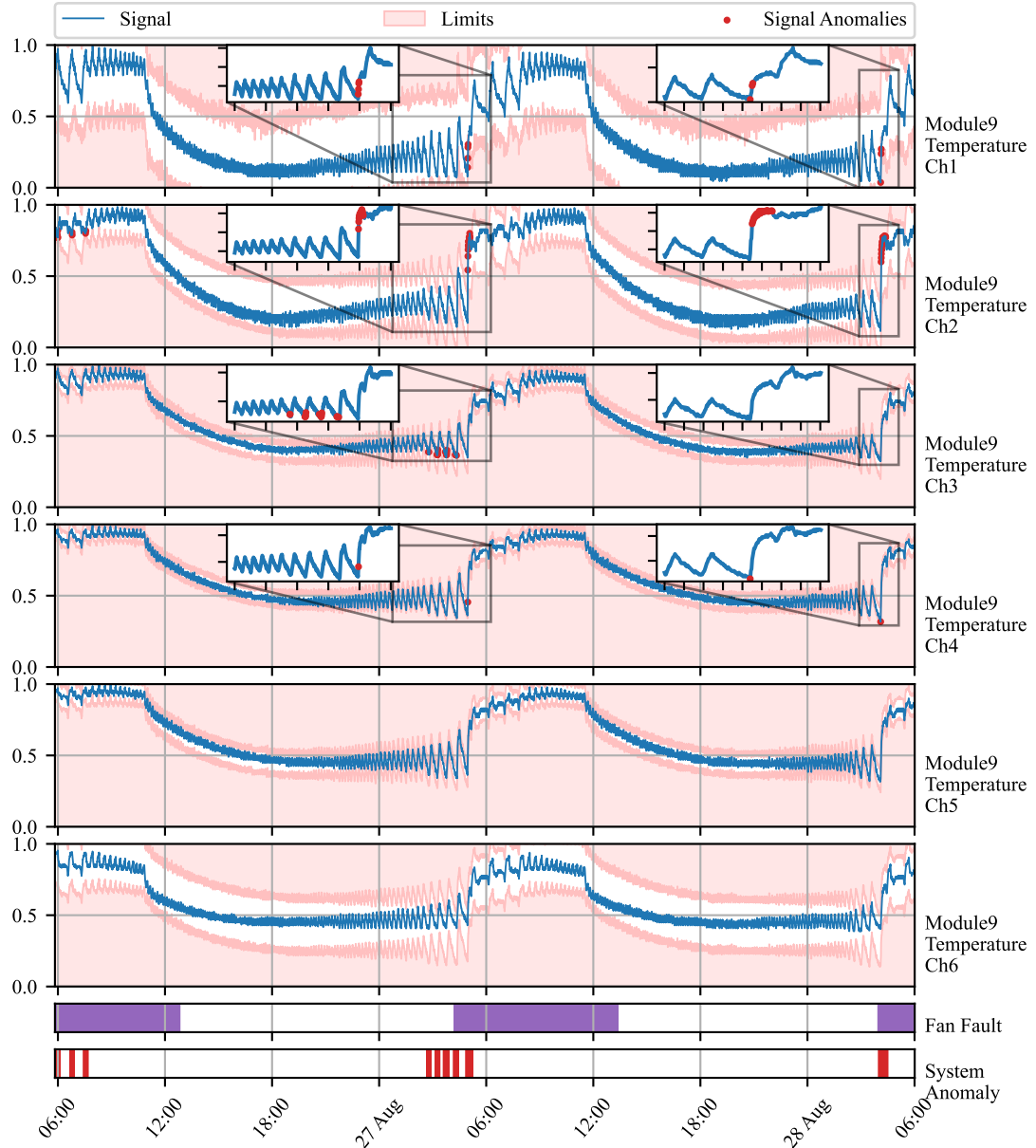


Figure 8: Time series of battery module 9 measurements (blue line). The y-axis renders the normalized deviations of temperature from an average of all modules. Signal anomalies are marked as red dots. The light red area represents an area out of dynamic operating limits. True fan faults are marked by purple bars. Green bars represent the times of changepoint detection. Red bars denote the period where any of the signals contained anomaly.

643 These methods are widely recognized for their iterative learning capabilities
644 on multivariate time-series data, making them suitable for anomaly detection
645 in dynamic systems, as previously discussed in the Introduction 1.3.

646 The comparison is based on the Skoltech Anomaly Benchmark (SKAB)
647 dataset, a real-world dataset with annotated labels distinguishing between
648 anomalous and normal observations (Katser and Kozitsin, 2020). SKAB
649 is used for this purpose, as no established benchmarking multivariate data
650 were found regarding energy storage systems similar to the ones studied in
651 Subsection 4.1 and Subsection 4.2. The SKAB dataset involves experiments
652 related to rotor imbalance, where various control actions and changes in
653 water volume are introduced to the system. It encompasses eight features
654 and exhibits both gradual and sudden drifts.

655 To ensure fairness in the benchmark, data preprocessing adheres to best
656 practices for each method. OC-SVM employs standard scaling, while HS-
657 Trees use normalization. Our proposed AID method requires no scaling.
658 Preprocessing is performed online, simulating a real production environment,
659 with running mean and variance for standard scaling and running peak-to-
660 peak distance for normalization, as supported by the online machine learning
661 library "river" (Montiel et al., 2021).

662 The optimal hyperparameters for both reference methods are found us-
663 ing Bayesian Optimization. Due to no further knowledge about the data
664 generating process, and equity in benchmark, the hyperparameters of our
665 proposed method were optimized using Bayesian Optimization as well. 20
666 steps of random exploration with 100 iterations of Bayesian Optimization
667 were used, increasing default values set in the Bayesian Optimization library,
668 to allow thorough exploration and increase the possibility of finding global
669 optima in each case (Nogueira, 2014). The hyperparameters are optimized
670 with the F1 score as a cost function first, to maximize both precision and
671 recall on anomalous samples.

672 As adaptation is required and anticipated within benchmark datasets,
673 the performance is evaluated iteratively, similarly to the operation after de-
674 ployment. The metric is updated with each new sample and its final value is
675 used to drive Bayesian Optimization. The performance is evaluated using the
676 best-performing model, found by Bayesian Optimization. The performance
677 of the proposed method is evaluated on the same data as the models are
678 optimized for.

679 Hyperparameter search ranges are specified, with values centered around
680 default library values for OC-SVM and HS-Trees. The ranges are inten-

681 tionally set wide to facilitate comprehensive exploration. The quantile filter
 682 threshold used in OC-SVM and HS-Trees aligns with the threshold used in
 683 AID. These hyperparameter ranges are presented in Table 1.

Table 1: Hyperparameter Ranges for Detection Algorithms

Algorithm	Hyperparameters	Default	Ranges
AID	Threshold	0.99735	(0.85, 0.99994)
	t_e	-	(150, 10000)
	t_a	t_e	(50, 2000)
	Grace Period	t_e	(50, 1000)
OC-SVM	Threshold	-	(0.85, 0.99994)
	Learning Rate	0.01	(0.005, 0.02)
HS-Trees	Threshold	-	(0.85, 0.99994)
	N Trees	10	(0, 20)
	Max Height	8	(2, 14)
	Window Size	250	(100, 400)

684 The results for models optimized for the F1 score are summarized in Ta-
 685 ble 2, which includes precision, recall, F1 score, and average latency. Macro
 686 values are enclosed in brackets, representing the mean of the metric for both
 687 anomalies and normal data. A perfect detection achieves 100% in each met-
 688 ric. According to the Scoreboard for various algorithms on SKAB’s Kaggle
 689 page, all iterative approaches perform comparably to the batch-trained iso-
 690 lation forest and autoencoder, validating the optimization process. Notably,
 691 the proposed AID method outperforms both reference methods in terms of
 692 F1 score, recall, and precision, despite having a 30-fold higher latency per
 693 sample. This highlights the scalability as a candidate for further develop-
 694 ment. Nevertheless, in this case, sampling of the benchmark data still offers
 695 enough time to deliver predictions with sufficient frequency.

696 Optimal hyperparameters found during Bayesian Optimization are de-
 697tailed in Table 3. None of the parameters are at the edge of the provided
 698 ranges, serving as necessary proof of ranges being broad enough. Never-
 699 theless, sufficient proof is not possible as multiple parameter ranges are not
 700 bounded by designed limits.

Table 2: Evaluation of models optimized for F1 score on SKAB dataset (Katser and Kozitsin, 2020). The best-performing model is highlighted in bold. Values in brackets represent macro values of the metric.

Algorithm	Precision [%]	Recall [%]	F1 [%]	Avg. Latency [ms]
AID	41 (59)	80 (59)	54 (53)	1.45
HS-Trees	36 (51)	74 (51)	48 (44)	0.05
OC-SVM	39 (54)	63 (54)	48 (52)	0.05

Table 3: Optimal hyperparameters of methods optimized for F1 score

Algorithm	Hyperparameters	Found
AID	Threshold	0.96442
	t_e	1136
	t_a	396
	Grace Period	546
OC-SVM	Threshold	0.86411
	Learning Rate	0.01956
HS-Trees	Threshold	0.99715
	N Trees	1
	Max Height	7
	Window Size	283

701 5. Conclusion

702 In this paper, we demonstrate the capacity of adaptive conditional probability distribution to model the normal operation of dynamic systems employing streaming IoT data and isolate the root cause of anomalies. AID 703 dynamically adapts to non-stationarity by updating multivariate Gaussian 704 distribution parameters over time. Additionally, self-supervision enhances 705 the model by protecting it from the effects of outliers and increasing the 706 speed of adaptation in response to autonomously detected changes in oper- 707 ation.

708 Our statistical model isolates the root causes of anomalies as extreme 709 deviations from the conditional means vector, considering spatial and tem- 710 poral effects encoded in features, as demonstrated in our case studies. This 711 approach establishes the system’s operational state by analyzing the dis- 712

714 tribution of signal measurements, computing the distance from the mean
715 of conditional probability, and setting dynamic operating limits based on
716 multivariate distribution parameters. Additionally, the detector alerts for
717 non-uniform sampling due to packet drops and sensor malfunctions. These
718 adaptable limits can be seamlessly integrated into SCADA architecture, en-
719 hancing context awareness and enabling plug-and-play compatibility with
720 existing infrastructure.

721 The ability to detect and identify anomalies in the system, isolate the
722 root cause of anomaly to specific signal or feature, and identify signal losses
723 is shown in two case studies on data from operated industrial-scale energy
724 storages. These case studies highlight the model’s ability to adapt, diag-
725 nose the root cause of anomalies, and leverage both physical models and
726 spatially distributed sensors. Unlike many anomaly detection approaches,
727 the proposed AID method does not require historical data or ground truth
728 information about anomalies, alleviating the general limitations of detection
729 methods employed in the energy industry.

730 The benchmark performed on industrial data indicates that our model
731 provides comparable results to other self-learning adaptable anomaly detec-
732 tion methods. This is an important property of our model, as it also allows
733 for root cause isolation.

734 AID represents a significant advancement in the safety and profitability
735 of evolving systems that utilize well-established SCADA architecture and
736 streaming IoT data. By providing dynamic operating limits, AID seamlessly
737 integrates with existing alarm mechanisms commonly employed in SCADA
738 systems. To the best of our knowledge, this study appears to be one of the
739 initial attempts to introduce a self-supervised approach for adaptive anomaly
740 detection and root cause isolation in SCADA-based systems utilizing IoT
741 data streams.

742 Future work on this method will include improvements to the change point
743 detection mechanism, reduction in latency for high-dimensional data, and
744 minimizing the false positive rate, which is a challenge for general plug-and-
745 play models. We will also explore the ability to operate with non-parametric
746 models, in contrast to Gaussian distribution.

747 Additional information

748 Our framework is openly accessible on GitHub at the following URL:
749 https://github.com/MarekWadinger/online_outlier_detection.

750 **CRediT authorship contribution statement**

751 **Marek Wadinger:** Conceptualization; Data curation; Formal analysis;
752 Investigation; Methodology; Resources; Software; Validation; Visualization;
753 Writing - original draft; and Writing - review & editing. **Michal Kvasnica:**
754 Conceptualization; Funding acquisition; Project administration; Resources;
755 Supervision; Validation.

756 **Declaration of Competing Interest**

757 The authors declare that they have no known competing financial inter-
758 ests or personal relationships that could have appeared to influence the work
759 reported in this paper.

760 **Acknowledgements**

761 This work was supported by the Horizon Europe [101079342]; the Slovak
762 Research and Development Agency [APVV-20-0261]; and the Scientific Grant
763 Agency of the Slovak Republic [1/0490/23].

764 **References**

- 765 Ahmad, S., Lavin, A., Purdy, S., Agha, Z., 2017. Unsuper-
766 vised real-time anomaly detection for streaming data. Neuro-
767 computing 262, 134–147. URL: <https://www.sciencedirect.com/science/article/pii/S0925231217309864>, doi:<https://doi.org/10.1016/j.neucom.2017.04.070>. online Real-Time Learning Strategies for
768 Data Streams.
- 771 Amarasinghe, K., Kenney, K., Manic, M., 2018. Toward explainable deep
772 neural network based anomaly detection, in: 2018 11th International Con-
773 ference on Human System Interaction (HSI), pp. 311–317. doi:[10.1109/HSI.2018.8430788](https://doi.org/10.1109/HSI.2018.8430788).
- 775 Amer, M., Goldstein, M., Abdennadher, S., 2013. Enhancing one-class sup-
776 port vector machines for unsupervised anomaly detection, in: Proceedings
777 of the ACM SIGKDD Workshop on Outlier Detection and Descrip-
778 tion, Association for Computing Machinery, New York, NY, USA. pp.
779 8–15. URL: <https://doi.org/10.1145/2500853.2500857>.

- 781 Barbosa Roa, N., Travé-Massuyès, L., Grisales-Palacio, V.H., 2019. Dy-
782 clee: Dynamic clustering for tracking evolving environments. Pat-
783 tern Recognition 94, 162–186. URL: <https://www.sciencedirect.com/science/article/pii/S0031320319301992>, doi:<https://doi.org/10.1016/j.patcog.2019.05.024>.
- 786 Bosman, H.H., Iacca, G., Tejada, A., Wörtche, H.J., Liotta, A., 2015. En-
787 sembles of incremental learners to detect anomalies in ad hoc sensor net-
788 works. Ad Hoc Networks 35, 14–36. URL: <https://www.sciencedirect.com/science/article/pii/S1570870515001481>, doi:<https://doi.org/10.1016/j.adhoc.2015.07.013>. special Issue on Big Data Inspired Data
790 Sensing, Processing and Networking Technologies.
- 791
- 792 Brito, L.C., Susto, G.A., Brito, J.N., Duarte, M.A.V., 2023. Fault diag-
793 nosis using explainable ai: A transfer learning-based approach for ro-
794 tating machinery exploiting augmented synthetic data. Expert Systems
795 with Applications 232, 120860. URL: <https://www.sciencedirect.com/science/article/pii/S0957417423013623>, doi:<https://doi.org/10.1016/j.eswa.2023.120860>.
- 796
- 797
- 798 Carletti, M., Masiero, C., Beghi, A., Susto, G.A., 2019. Explainable machine
799 learning in industry 4.0: Evaluating feature importance in anomaly detec-
800 tion to enable root cause analysis, in: 2019 IEEE International Conference
801 on Systems, Man and Cybernetics (SMC), pp. 21–26. doi:[10.1109/SMC.2019.8913901](https://doi.org/10.1109/SMC.2019.8913901).
- 802
- 803 Chandola, V., Banerjee, A., Kumar, V., 2009. Anomaly detection: A sur-
804 vey. ACM Comput. Surv. 41. URL: <https://doi.org/10.1145/1541880.1541882>, doi:[10.1145/1541880.1541882](https://doi.org/10.1145/1541880.1541882).
- 805
- 806 Cook, A.A., Misirlı, G., Fan, Z., 2020. Anomaly detection for iot time-
807 series data: A survey. IEEE Internet of Things Journal 7, 6481–6494.
808 doi:[10.1109/JIOT.2019.2958185](https://doi.org/10.1109/JIOT.2019.2958185).
- 809
- 810 Du, X., Chen, J., Yu, J., Li, S., Tan, Q., 2024. Generative adversarial nets
811 for unsupervised outlier detection. Expert Systems with Applications 236,
812 121161. URL: <https://www.sciencedirect.com/science/article/pii/S0957417423016639>, doi:<https://doi.org/10.1016/j.eswa.2023.121161>.
- 813

- 814 Fan, C., Sun, Y., Zhao, Y., Song, M., Wang, J., 2019. Deep learning-
815 based feature engineering methods for improved building energy predic-
816 tion. Applied Energy 240, 35–45. URL: <https://www.sciencedirect.com/science/article/pii/S0306261919303496>, doi:<https://doi.org/10.1016/j.apenergy.2019.02.052>.
- 819 Genz, A., 2000. Numerical computation of multivariate normal probabili-
820 ties. Journal of Computational and Graphical Statistics 1. doi:[10.1080/10618600.1992.10477010](https://doi.org/10.1080/10618600.1992.10477010).
- 822 Gözüaçık, Ö., Can, F., 2021. Concept learning using one-class classi-
823 fiers for implicit drift detection in evolving data streams. Artificial
824 Intelligence Review 54, 3725–3747. URL: <https://doi.org/10.1007/s10462-020-09939-x>, doi:[10.1007/s10462-020-09939-x](https://doi.org/10.1007/s10462-020-09939-x).
- 826 Huang, J., Cheng, D., Zhang, S., 2023. A novel outlier detecting algorithm
827 based on the outlier turning points. Expert Systems with Applications 231,
828 120799. URL: <https://www.sciencedirect.com/science/article/pii/S0957417423013015>, doi:<https://doi.org/10.1016/j.eswa.2023.120799>.
- 831 Iglesias Vázquez, F., Hartl, A., Zseby, T., Zimek, A., 2023. Anomaly detec-
832 tion in streaming data: A comparison and evaluation study. Expert Sys-
833 tems with Applications 233, 120994. URL: <https://www.sciencedirect.com/science/article/pii/S0957417423014963>, doi:<https://doi.org/10.1016/j.eswa.2023.120994>.
- 836 Katser, I.D., Kozitsin, V.O., 2020. Skoltech anomaly benchmark
837 (skab). <https://www.kaggle.com/dsv/1693952>. doi:[10.34740/KAGGLE/DSV/1693952](https://doi.org/10.34740/KAGGLE/DSV/1693952).
- 839 Kejariwal, A., 2015. Introducing practical and ro-
840 bust anomaly detection in a time series. URL:
841 https://blog.twitter.com/engineering/en_us/a/2015/introducing-practical-and-robust-anomaly-detection-in-a-time-series.
- 843 Krawczyk, B., Woźniak, M., 2015. One-class classifiers with incre-
844 mental learning and forgetting for data streams with concept drift.
845 Soft Computing 19, 3387–3400. URL: <https://doi.org/10.1007/s00500-014-1492-5>.

- 847 Laptev, N., Amizadeh, S., Flint, I., 2015. Generic and scalable frame-
848 work for automated time-series anomaly detection, in: Proceedings of
849 the 21th ACM SIGKDD International Conference on Knowledge Discov-
850 ery and Data Mining, Association for Computing Machinery, New York,
851 NY, USA. pp. 1939–1947. URL: <https://doi.org/10.1145/2783258.2788611>, doi:10.1145/2783258.2788611.
- 853 Li, J., Liu, Z., 2024. Attribute-weighted outlier detection for mixed
854 data based on parallel mutual information. Expert Systems with
855 Applications 236, 121304. URL: <https://www.sciencedirect.com/science/article/pii/S0957417423018067>, doi:<https://doi.org/10.1016/j.eswa.2023.121304>.
- 858 Liu, B., Xiao, Y., Yu, P.S., Cao, L., Zhang, Y., Hao, Z., 2014. Uncertain
859 one-class learning and concept summarization learning on uncertain data
860 streams. IEEE Transactions on Knowledge and Data Engineering 26, 468–
861 484. doi:10.1109/TKDE.2012.235.
- 862 Lyu, Y., Li, W., Wang, Y., Sun, S., Wang, C., 2020. Rmhsforest: Relative
863 mass and half-space tree based forest for anomaly detection. Chinese Jour-
864 nal of Electronics 29, 1093–1101. doi:<https://doi.org/10.1049/cje.2020.09.010>.
- 866 Miao, X., Liu, Y., Zhao, H., Li, C., 2019. Distributed online one-class support
867 vector machine for anomaly detection over networks. IEEE Transactions
868 on Cybernetics 49, 1475–1488. doi:10.1109/TCYB.2018.2804940.
- 869 Mishra, S., Datta-Gupta, A., 2018. Chapter 3 - distributions and models
870 thereof, in: Mishra, S., Datta-Gupta, A. (Eds.), Applied Statistical
871 Modeling and Data Analytics. Elsevier, pp. 31–67. URL: <https://www.sciencedirect.com/science/article/pii/B9780128032794000031>,
873 doi:<https://doi.org/10.1016/B978-0-12-803279-4.00003-1>.
- 874 Montiel, J., Halford, M., Mastelini, S.M., Bolmier, G., Sourty, R., Vaysse,
875 R., Zouitine, A., Gomes, H.M., Read, J., Abdessalem, T., Bifet, A., 2021.
876 River: machine learning for streaming data in python. Journal of Ma-
877 chine Learning Research 22, 1–8. URL: <http://jmlr.org/papers/v22/20-1380.html>.

- 879 Nguyen, Q.P., Lim, K.W., Divakaran, D.M., Low, K.H., Chan, M.C., 2019.
880 Gee: A gradient-based explainable variational autoencoder for network
881 anomaly detection, in: 2019 IEEE Conference on Communications and
882 Network Security (CNS), pp. 91–99. doi:10.1109/CNS.2019.8802833.
- 883 Nogueira, F., 2014. Bayesian Optimization: Open source constrained
884 global optimization tool for Python. URL: <https://github.com/fmfn/BayesianOptimization>.
- 885 Pannu, H.S., Liu, J., Fu, S., 2012. Aad: Adaptive anomaly detection system
886 for cloud computing infrastructures, in: 2012 IEEE 31st Symposium on
887 Reliable Distributed Systems, pp. 396–397. doi:10.1109/SRDS.2012.3.
- 888 Ruff, L., Kauffmann, J.R., Vandermeulen, R.A., Montavon, G., Samek, W.,
889 Kloft, M., Dietterich, T.G., Müller, K.R., 2021. A unifying review of deep
890 and shallow anomaly detection. Proceedings of the IEEE 109, 756–795.
891 doi:10.1109/JPROC.2021.3052449.
- 892 Salehi, M., Rashidi, L., 2018. A survey on anomaly detection in evolving
893 data: [with application to forest fire risk prediction]. SIGKDD Explor.
894 Newsl. 20, 13–23. URL: <https://doi.org/10.1145/3229329.3229332>,
895 doi:10.1145/3229329.3229332.
- 896 Stauffer, T., Chastain-Knight, D., 2021. Do not let your safe oper-
897 ating limits leave you s-o-l (out of luck). Process Safety Progress
898 40, e12163. URL: <https://aiche.onlinelibrary.wiley.com/doi/abs/10.1002/prs.12163>,
899 doi:<https://doi.org/10.1002/prs.12163>, arXiv:<https://aiche.onlinelibrary.wiley.com/doi/pdf/10.1002/prs.12163>.
- 900 Steenwinckel, B., 2018. Adaptive anomaly detection and root cause analy-
901 sis by fusing semantics and machine learning, in: Gangemi, A., Gentile,
902 A.L., Nuzzolese, A.G., Rudolph, S., Maleshkova, M., Paulheim, H., Pan,
903 J.Z., Alam, M. (Eds.), The Semantic Web: ESWC 2018 Satellite Events,
904 Springer International Publishing, Cham. pp. 272–282.
- 905 Steenwinckel, B., De Paepe, D., Vanden Hautte, S., Heyvaert, P., Bente-
906 frit, M., Moens, P., Dimou, A., Van Den Bossche, B., De Turck, F.,
907 Van Hoecke, S., Ongena, F., 2021. Flags: A methodology for adap-
908 tive anomaly detection and root cause analysis on sensor data streams
909 by fusing expert knowledge with machine learning. Future Generation
910 Computer Systems 160, 102–116. doi:10.1016/j.future.2021.102–116.
- 911

- 912 Computer Systems 116, 30–48. URL: <https://www.sciencedirect.com/science/article/pii/S0167739X20329927>, doi:<https://doi.org/10.1016/j.future.2020.10.015>.
- 915 Talagala, P.D., Hyndman, R.J., Smith-Miles, K., 2021. Anomaly
916 detection in high-dimensional data. Journal of Computational
917 and Graphical Statistics 30, 360–374. URL: <https://doi.org/10.1080/10618600.2020.1807997>,
918 doi:[10.1080/10618600.2020.1807997](https://doi.org/10.1080/10618600.2020.1807997),
919 arXiv:<https://doi.org/10.1080/10618600.2020.1807997>.
- 920 Tartakovsky, A.G., Polunchenko, A.S., Sokolov, G., 2013. Efficient computer
921 network anomaly detection by changepoint detection methods. IEEE Journal
922 of Selected Topics in Signal Processing 7, 4–11. doi:[10.1109/JSTSP.2012.2233713](https://doi.org/10.1109/JSTSP.2012.2233713).
- 924 Wadinger, M., Kvasnica, M., 2023. Real-time outlier detection with dynamic
925 process limits, in: 2023 24th International Conference on Process Control
926 (PC), pp. 138–143. doi:[10.1109/PC58330.2023.10217717](https://doi.org/10.1109/PC58330.2023.10217717).
- 927 Welford, B.P., 1962. Note on a method for calculating corrected sums of
928 squares and products. Technometrics 4, 419–420. doi:[10.1080/00401706.1962.10490022](https://doi.org/10.1080/00401706.1962.10490022).
- 930 Wetzig, R., Gulenko, A., Schmidt, F., 2019. Unsupervised anomaly alerting
931 for iot-gateway monitoring using adaptive thresholds and half-space
932 trees, in: 2019 Sixth International Conference on Internet of Things: Sys-
933 tems, Management and Security (IOTSMS), pp. 161–168. doi:[10.1109/IOTSMS48152.2019.8939201](https://doi.org/10.1109/IOTSMS48152.2019.8939201).
- 935 Wu, H., He, J., Tömösközi, M., Xiang, Z., Fitzek, F.H., 2021. In-network
936 processing for low-latency industrial anomaly detection in softwarized net-
937 works, in: 2021 IEEE Global Communications Conference (GLOBECOM),
938 pp. 01–07. doi:[10.1109/GLOBECOM46510.2021.9685489](https://doi.org/10.1109/GLOBECOM46510.2021.9685489).
- 939 Wu, Z., Yang, X., Wei, X., Yuan, P., Zhang, Y., Bai, J., 2024. A self-
940 supervised anomaly detection algorithm with interpretability. Expert Sys-
941 tems with Applications 237, 121539. URL: <https://www.sciencedirect.com/science/article/pii/S0957417423020419>, doi:<https://doi.org/10.1016/j.eswa.2023.121539>.

- 944 Yamanishi, K., Takeuchi, J.i., 2002. A unifying framework for detecting outliers
945 and change points from non-stationary time series data, in: Proceedings
946 of the Eighth ACM SIGKDD International Conference on Knowledge
947 Discovery and Data Mining, Association for Computing Machinery, New
948 York, NY, USA. pp. 676–681. URL: <https://doi.org/10.1145/775047.775148>, doi:10.1145/775047.775148.
- 950 Yamanishi, K., Takeuchi, J.i., Williams, G., Milne, P., 2004. On-line
951 unsupervised outlier detection using finite mixtures with discounting
952 learning algorithms. *Data Mining and Knowledge Discovery* 8, 275–
953 300. URL: <https://doi.org/10.1023/B:DAMI.0000023676.72185.7c>,
954 doi:10.1023/B:DAMI.0000023676.72185.7c.
- 955 Yang, W.T., Reis, M.S., Borodin, V., Juge, M., Roussy, A., 2022. An
956 interpretable unsupervised bayesian network model for fault detection
957 and diagnosis. *Control Engineering Practice* 127, 105304. URL: <https://www.sciencedirect.com/science/article/pii/S0967066122001502>,
958 doi:<https://doi.org/10.1016/j.conengprac.2022.105304>.
- 960 Zhang, K., Chen, J., Lee, C.G., He, S., 2024. An unsupervised spatiotemporal
961 fusion network augmented with random mask and time-relative
962 information modulation for anomaly detection of machines with
963 multiple measuring points. *Expert Systems with Applications* 237,
964 121506. URL: <https://www.sciencedirect.com/science/article/pii/S0957417423020080>, doi:<https://doi.org/10.1016/j.eswa.2023.121506>.
- 967 Zhang, X., Shi, J., Huang, X., Xiao, F., Yang, M., Huang, J., Yin,
968 X., Sohail Usmani, A., Chen, G., 2023. Towards deep probabilistic
969 graph neural network for natural gas leak detection and localization
970 without labeled anomaly data. *Expert Systems with Applications* 231,
971 120542. URL: <https://www.sciencedirect.com/science/article/pii/S0957417423010448>, doi:<https://doi.org/10.1016/j.eswa.2023.120542>.